Parameter identification of micron-sized freestanding stretchable electronic interconnects using integrated digital height correlation

OPEN ACCESS
IOP Publishing
Measurement Science and Technology
Meas. Sci. Technol. **32** (2021) 064001 (15pp)
https://doi.org/10.1088/1361-6501/abd513

Parameter identification of micron-sized freestanding stretchable electronic interconnects using integrated digital height correlation

S M Kleinendorst, S Shafqat, M G D Geers and J P M Hoefnagels

Department of Mechanical Engineering, Eindhoven University of Technology, Gemini-Zuid 4.122, 5600MB Eindhoven, The Netherlands

E-mail: j.p.m.hoefnagels@tue.nl

Received 11 July 2020, revised 23 November 2020
Accepted for publication 17 December 2020
Published 30 March 2021

Abstract

For the development of reliable stretchable electronic systems, it is essential to comprehend and predict their mechanical behavior. It is important to test and analyze original as-processed samples, as opposed to standard tests on bulk material. Dedicated analysis methods are necessary for obtaining the material properties from the tests, as complex 3D deformations complicate the use of existing methods. This paper presents an integrated digital height correlation (IDHC) method for the mechanical characterization of a recently developed ultra-stretchable freestanding interconnect. Height maps from an out-of-plane loading experiment are correlated to a numerical model, with the aim to identify the material parameters in the plastic regime. The IDHC method is tested on a virtual test case, where it is shown that the algorithm converges for the considered three plasticity parameters. For the real experiment, simultaneous correlation of all three parameters is not possible due to an inherently flat residual landscape with many local minima. However, the initial yield strength and hardening exponent were still identified and estimated at 225–300 MPa and 0.15–0.2 respectively. Despite the moderate accuracy of the identification, the potency of the IDHC method for this extremely challenging case of micron-sized delicate freestanding stretchable electronic interconnects is demonstrated.

Keywords: parameter identification, stretchable electronics, integrated digital height correlation

(Some figures may appear in colour only in the online journal)

1. Introduction

Stretchable electronics is an emerging field of research, with applications mainly in the biomedical field, used to integrate traditionally rigid electronics with soft biological tissue [1–4]. In order to develop reliable systems that are safe to use in this biological environment, it is important to characterize the mechanical behavior of the stretchable electronics. Miniaturization of the stretchable electronics leads to size effects, which restricts assessing the material behavior *a priori* [5–7]. Moreover, the processing history might affect the material properties, as well as the loading conditions triggering different deformation modes [8]. Therefore, it is essential to perform tests on original as-processed samples of the interconnects in order to characterize their mechanical behavior with all these effects incorporated.

The design of stretchable electronics generally follows one of two different approaches [9–11]: either to use conductive materials that are stretchable [12] or to make structural designs for stretchable interconnects from a conductive material with low intrinsic stretchability [13]. The in this work considered stretchable electronic interconnect is a design according to the second approach. Examples of such designs include wavy silicon ribbons or arches [14, 15], serpentine or horseshoe

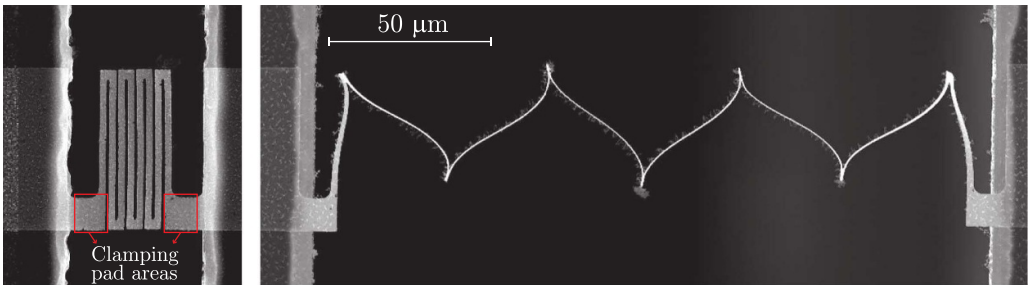

Figure 1. (a) The freestanding ultra-stretchable ROPE interconnect design, consisting of a number of rectangular beams. (b) The interconnect in stretched state; beam members rotate out-of-plane and bend to align with and elongate along the stretch direction.

shaped interconnects [16–19], fractal designs [20, 21] and origami [22, 23] and kirigami [24, 25] inspired designs.

Recently, a freestanding ultra-stretchable interconnect, also called the ROPE (Rotation Out-of-Plane Elongation) interconnect, was developed, see figure 1, which exploits full three-dimensional freedom up to a reversible stretchability of about 2000% [26]. A strong strengthening effect was observed; i.e. by roughly comparing experimental results to numerical simulations, using a standard elasto-plasticity model, a yield strength of roughly ten times higher than the value for bulk aluminum (from which the interconnect is fabricated) was estimated. This observation is important for the stretching behavior of these interconnects and also interesting from a scientific point of view. The objective of this paper is therefore to quantitatively determine the plastic behavior of these interconnects.

The interconnects are designed to be highly compliant, which makes it difficult to employ a (uniaxial) tensile experiment to determine the material properties, as the forces are too low to be measured in a sufficiently accurate manner. Alternatively, a full-field method such as Digital Image Correlation (DIC) may be used to characterize the kinematics of the structure. Moreover, when an integrated approach is used, i.e. when the image correlation is complemented by a numerical model, the (material) parameters in this model may be identified directly [27–29]. However, standard DIC techniques only provide the in-plane displacement field, whereas the considered interconnects deform predominantly out of their plane, see figure 1(b). In the literature, stereo-DIC (sometimes called '3D' DIC), which uses a setup of two cameras under an angle, has been applied to measure the three-dimensional deformation field of electronic packages, however, the field of view of such 2-camera setups is at least tens of millimeters [30]. A '3D DIC' method that is more suited for our problem but less known is that of Digital Height Correlation (DHC), in which surface height profiles instead of grey-scale images are correlated to obtain the full three-dimensional displacement field inside the field of view, i.e. both the in-plane and out-of-plane surface displacements of the considered specimen [31–36]. The strength of DIC lies in the fact that surface height profiles with an out-of-plane resolution of approximately one nanometer and a field of view of tens of micrometers (instead of millimeters) are readily measured using a range of commercially available (metrological) optical surface profilometers. This makes the DHC technique based on such high-resolution surface height profiles ideally suited for measuring the in-plane and out-of-plane deformations in the free-standing stretchable interconnects. Therefore, in this paper, an *integrated* digital *height* correlation (IDHC) method is proposed to directly identify the (plastic) material parameters from an *in situ* experiment on freestanding ultra-stretchable interconnects underneath an optical surface profilometer.

The IDHC method requires that the surface of interest stays in view during the experiment. Hence, it is not possible to load the structure by in-plane stretching as done in [26], because the beam members of the interconnect rotate out-of-view to align with the stretch direction, see figure 1(b). Although the outer beam members twist to accommodate rotation of the other beams, the majority of the beams deform in pure bending mode after rotation. This mode can also be triggered by loading the interconnect in the out-of-plane direction, while the beam surfaces stay in view [37].

For parameter identification methods, such as the IDHC method, it is essential that the accompanying model, here a finite element (FE) model, mirrors the experiment as close as possible. Especially the boundary conditions are influential [38, 39]. Moreover, in the particular case of miniature freestanding stretchable interconnects, also the initial geometry, which is curved due to residual stresses from manufacturing, requires special attention. Therefore, the initial geometry of the free-standing stretchable interconnect in the FE model will be extracted from the measured height profile in the reference configuration. Furthermore, a global DHC method will be used to extract the complete evolution of the 3D displacement of the clamping pad areas, see figure 1(a), which is employed as boundary conditions in the FE model to accurately take into account all experimental discrepancies in the out-of-plane cyclic load case to which the interconnect will be subjected.

The paper is organized as follows: first the methodology is explained in section 2, which consists of the experimental details, discussion of the integrated digital height correlation algorithm and some aspects of the FE model. In section 3, the analysis of the experiment is presented. First a DHC algorithm is employed for preliminary analysis of the boundary conditions for the FE model, after which the IDHC algorithm is tested by means of a virtual test. Subsequently, the IDHC

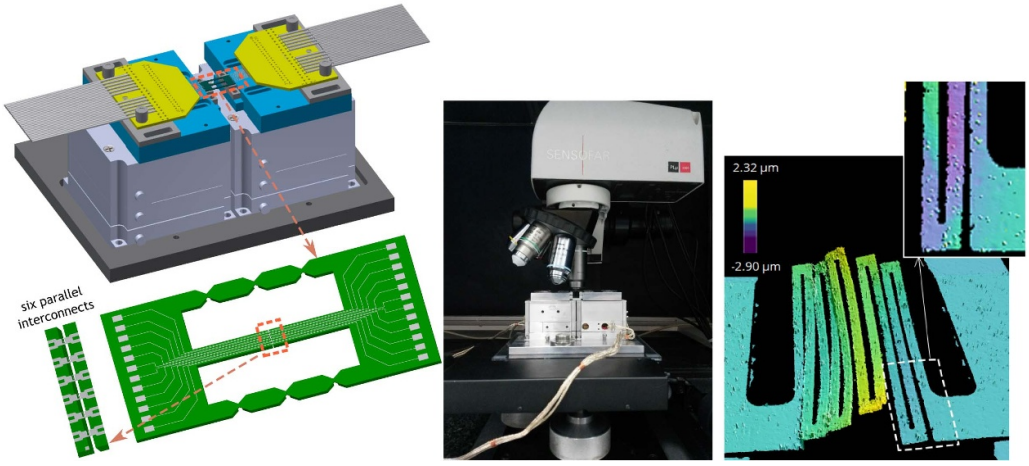

(a) Tensile stage and specimen chip (b) Total setup with confocal microscope (c) Measured specimen

Figure 2. (a) Rendering of the piezoelectric tensile stage and the specially designed chip that contains the delicate stretchable interconnect samples. The sacrificial support beams on both sides of the interconnect array, that allow for secure handling and alignment of the specimen, can be broken at the notches after the chip has been securely clamped in the tensile device, without causing a pre-load. (b) The tensile stage placed underneath the confocal optical microscope, which allows for capturing height maps of the interconnect samples during the experiment. (c) 3D rendering of the measured height map and overlay of the height map on a microscopic image of the specimen (inset), in which the pattern features can be seen.

algorithm is applied to the experimental data. Finally, conclusions are drawn in section 4.

2. Methodology

In this section the methodology for the analysis of the freestanding stretchable interconnects is explained.

2.1. Experiment

In order to identify the mechanical properties of the freestanding stretchable electronic interconnects an experiment is performed in which one of the main deformation modes of these structures is triggered: bending of the interconnect beams. The specimen has a planar design of slender, rectangular beams; the interconnect in this experiment consists of ten beams. The interconnect is embedded in a specially designed chip that allows for meticulous handling of the sensitive samples [26]. To be able to perform a DIC analysis on the samples, a distinct pattern needs to be present. In this case pattern application is complicated, as it is not possible to apply many techniques known from literature [40–42]. Indeed, pattern application using a fluid or plasma is prohibited, because even small forces resulting from contact with a fluid or charging due to plasma lead to plastic deformation of the highly delicate samples or stiction of the interconnect beams to each other or the substrate. The only possibility for pattern application is a flow of dry particles that individually attach to the interconnect. This was realized by applying silica nano-particles (300 nm) on the interconnect by means of a dried micro-mist application technique. Yet, only a sparse pattern, with only a few particles over the beam length could be accomplished due to the highly delicate nature of the freestanding interconnects [37]. However, it is expected that plasticity is mainly characterized by a change in curvature of the beams and that this sparse pattern is sufficient to capture this effect. The methods adopted in this work to identify the mechanical behavior and properties from this experiment are *global* DIC methods (see next section). These types of methods entail regularization of the total region of interest at once, as opposed to *local* methods, in which the region of interest is divided in (uncoupled) subsets. Local methods would be impossible to apply on such a sparse pattern, but due to the strong global regularization in global methods, it is still possible to identify the mechanical behavior and properties from the height maps, despite the poor pattern quality.

A lab-built dedicated tensile stage for the micron-sized samples is used to load the interconnect structure, see figure 2. This tensile stage consists of two high-resolution piezoelectric nano-positioning stages, each consisting of a stacked assembly of three stages, one for each degree of freedom (x, y and z translation). This design makes it possible to actuate along all three axes, and enables complex multi-axial loading. The test chip containing the stretchable interconnect specimen is clamped on either side to these stages, using UV curable glue, such that the top surface of the test chip is free to fit underneath a microscope lens with small working distance. The specimen is loaded in the out-of-plane direction, by moving the clamping pads on either side of the interconnect by a prescribed displacement, enabled by the internal displacement sensors and control loop of the tensile device. After loading, the specimen is unloaded again, i.e. the clamping pads are returned to their original position. This process is repeated, while the displacement-controlled load increases incrementally.

Topographical images are captured during the experiment by means of a confocal optical microscope (Sensofar S Neox,

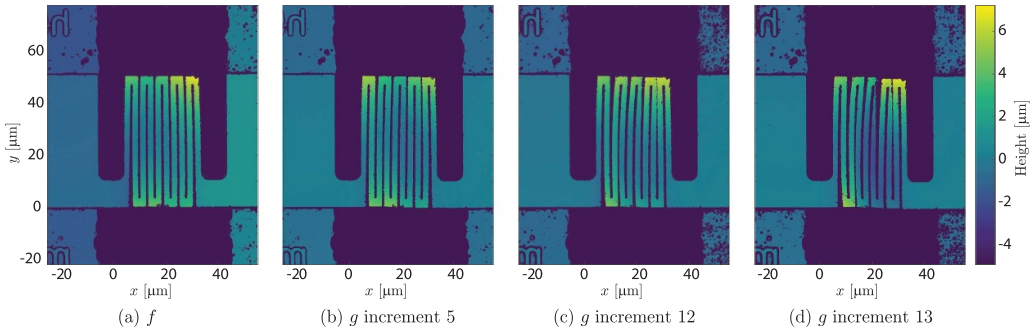

(a) f (b) g increment 5 (c) g increment 12 (d) g increment 13

Figure 3. Height maps captured during the experiment for a selection of loading increments. The reference image, f, of the undeformed configuration is shown, along with three deformed images g, each obtained after a number of incremental loading-unloading cycles (named here increments).

150× magnification lens with a numerical aperture of 0.95 and working distance 300 µm). In the loaded situation the beams are bend to a steep angle with respect to the microscope, which makes it impossible to capture the height map with the profilometer, see the image marked 'topographies extended state' in figure 4. Therefore, the experiment is designed such that images are taken in the unloaded configuration after each loading step, see figure 3. This is a justified approach, since the objective of the experiment is to identify the material properties that represent the plastic regime, and plastic deformation will also be reflected in the unloaded state, as observed in figures 3(c) and (d). The complete experimental procedure is described in more detail in [37].

Note that during the design of the coupled experimental-numerical methodology the free-standing interconnects were expected to be highly stretchable but still much less than observed in figure 3. As a result of this extreme stretchability, no plasticity is visible in figure 3(b), corresponding to a relative vertical displacement of the clamping pads of ∼10 µm, even though this is already beyond half of the 200 µm range of the experimental setup. Moreover, from later analysis, it was also realized that the visual deformation in figures 3(c) and (d) is, for a large part, not caused by plasticity but by small in-plane shifts of the clamping pads after returning to the unloaded state in combination with the initially curved surface due to residual stresses. Therefore, the degree of out-of-plane deformation after unloading due to plasticity is limited (due to the experimental setup) compared to the combined effects of the residual stress-induced and clamping pad shifts-induced out-of-plane deformation. These experimental complications make identification of the plastic material parameters of these ultra-stretchable free-standing interconnects highly challenging, placing large requirements on the robustness of the parameter identification methodology.

2.2. Integrated digital height correlation

An integrated digital height correlation (IDHC) algorithm is used to analyze the material properties of the stretchable electronic interconnects. This is an extension of integrated digital image correlation (IDIC), where the correlation of the images is combined with finite element (FE) simulations [27–29], see figure 4. The calculated displacements following the FE simulation are used to back-deform the images of the deformed sample, in order to get an optimal match with the reference image of the specimen in undeformed configuration. The difference between the images, i.e. the residual, is minimized iteratively. The parameters in the FE model are the degrees of freedom (DoFs) in the correlation, therefore usually this approach is employed if the objective of the experiment is to identify material properties. In the *height* correlation method the images are not grayscale images of the specimen, but topographic height profiles of the sample's surface [35, 36]. Hence, not only the in-plane displacement is tracked, but simultaneously also the out-of-plane deformation is included in the correlation.

The minimization of the residual is a non-linear problem, which is commonly solved iteratively using a Newton–Raphson scheme [29, 43]. In this scheme the search direction is determined by the image gradients and the sensitivity of the displacement field (following from the finite element simulations and evaluated at the pixel coordinates) towards the degrees of freedom (material parameters in the finite element model). Finite differences are used to calculate this sensitivity, where the parameters are perturbed by a small amount to determine the effect on the displacement field. The size of this perturbation is a calculation parameter that needs to be set and in this work it was chosen to be 1 thousands of the parameter value. Furthermore, a convergence criterion needs to be set. Commonly, the Euclidean vector norm of the right hand side member of the problem is used for this, which contains the residual that is minimized. Here, the criterion is set to 1×10^{-6}.

In DIC algorithms usually a region of interest (ROI) is selected in the reference image, such that the pattern features in the selected region do not move out of view in the deformed images and to make sure nodal displacements from the FE simulation are available in the entire region of interest. In this case the region of interest is not a rectangular area, but it is based on the shape of the interconnect, as defined in the finite element model. Furthermore, the measured height data contains many not-a-number (NaN) values, especially around the edges of the structure, since the profilometer does not measure the heights at steep gradients or edges. These values

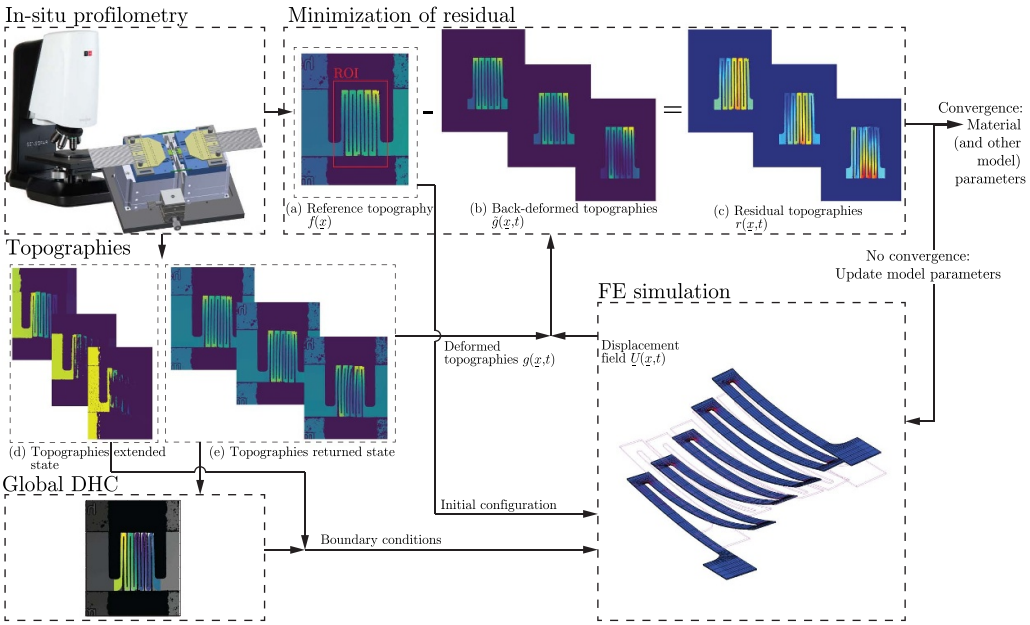

Figure 4. Schematic illustration of the integrated digital height correlation method: the core of the algorithm is the minimization of the residual (c), which is a measure for the optimality of the parameters of the FE model. The topographies captured during the experiment ((a), (d) and (e)) are not only used for the correlation itself, but also to determine boundary conditions required for the FE model. The dynamic range of topographies (a), (b) and (e) is ∼− 5 to 7 µm. The dynamic range for the first and last topography in (d) is respectively ∼[−30 40] and [−100 120] µm.

proliferate during the interpolation step, which is required to determine the back-deformed images [44], and destructively influence the correlation. Therefore, a mask is defined to discard the pixels containing NaN values, both in the reference topography and the back-deformed topographies. This mask is reset and updated adaptively during the iterations to prevent an unnecessary high number of discarded pixels.

2.3. *Finite element model*

For IDHC a numerical model is required that represents the experiment. It is therefore important that the model resembles the physical reality as close as possible [38]. To this end, the stretchable interconnect structure with ten beams is modeled conforming the geometry of the design supplied to the manufacturer of the samples. Slight deviations from the design in the real samples, e.g. slightly round finishes of the corners, are disregarded, but this is justified as they fall outside the region of interest for correlation, since the height measurements at the edges of the sample are not reliable.

One of the main challenges in the model is to obtain the exact reference configuration of the experiment, in which the beams are curved due to residual stresses from processing. To this end, the straight modeled mesh is overlayed on the topographic image of the reference situation and for each node the measured height at its location is translated to this node. However, because of measurement noise (and pattern features), this would result in a non-smooth surface that would unrealistically influence the kinematics in the simulation. To smoothen the curved surface, a regression is made through the measured data, see figure 5, where a second-order polynomial is used along the length of the beams and a first-order polynomial in the width direction. The hinges and clamping areas are smoothed separately, using constraints to connect them appropriately to the beams, ensuring C^1 continuity across the connecting lines.

Also the in-plane alignment of the reference configuration, and particularly the lateral bending of the four most right beams, needs to be accounted for in the FE model. This lateral bending is also attributed to the residual stress. As no images of the unwarped interconnect (before chemical etching of the sacrificial layer to release the interconnects) are available, which could be correlated by a DHC method to the topography of the warped interconnect in order to determine the exact in- and out-of-plane deformations due to the residual stresses, the in-plane displacement (from a perfectly straight configuration to the measured situation) can now only be determined manually. This is done at the corners of the hinges and prescribed in the simulation. The resulting initial configuration, see figure 6, is assumed to be stress-free, because the curved shape is precisely the result of the fact that the freestanding structure can almost completely relax the residual stresses that were acting on it.

The material model used in the simulation is elasto-plastic, where Hooke's law for elasticity is used and the Von Mises yield criterion [45], with a rate power law model for (isotropic) hardening:

$$\sigma_y = \sigma_{y0} + A\bar{\varepsilon}_p^m, \tag{1}$$

where σ_y is the evolving yield stress, $\bar{\varepsilon}_p$ is the equivalent plastic strain, σ_{y0} the initial yield strength, A a hardening coefficient and m the hardening exponent. The latter three are

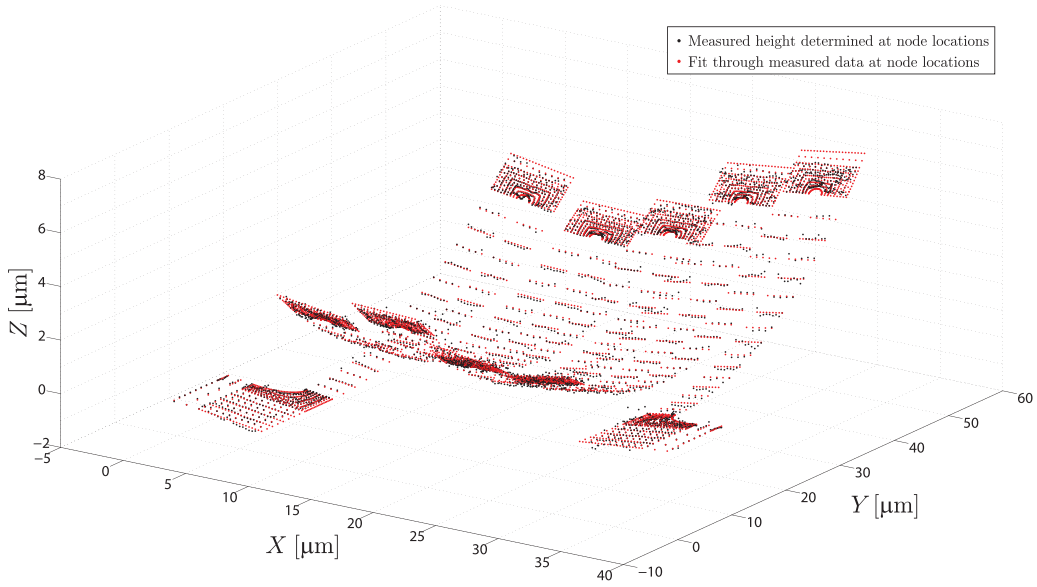

Figure 5. Three-dimensional locations of the nodes of the FE model, based on the measured height data (black dots) and a regression through this data (red dots) to smoothen the surface from measurement artifacts (note that the axes are not equal for visualization purposes).

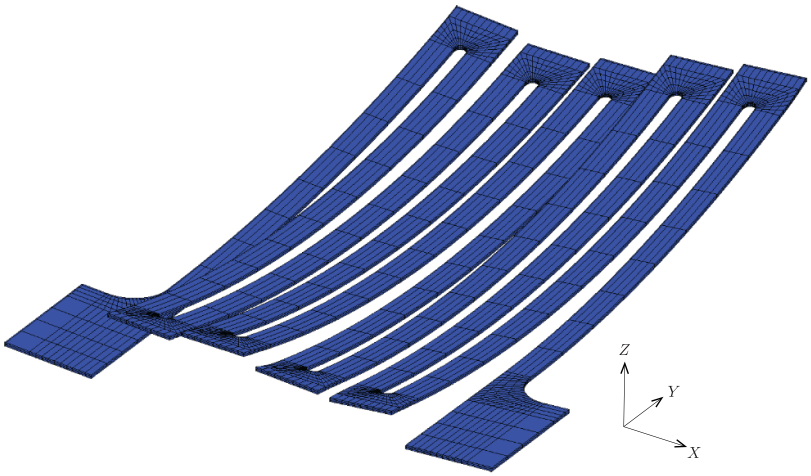

Figure 6. FE model of the stretchable interconnect geometry with 10 beams, in the curved initial configuration.

unknown parameters and hence the objective for the identification using the IDHC method. Especially the initial yield strength is interesting to investigate, as it was found by [26] to be influenced drastically by size effects due to the small dimensions and processing conditions (up to ten times its value for the corresponding bulk material).

The boundary conditions in the model are also an important input that need to be in close agreement with the experimental conditions. During the experiment, topographies are measured in both the extended and returned state for all increments. The topographies in the extended state are not useful for correlation, because of the large inaccuracies in the measured height values in the presence of high gradients, see figure 4. The pads, however, are an almost flat area on which the height values are reliable and therefore used to define the boundary conditions in the extended state. For the boundary conditions in the returned state, the global DHC algorithm from [35] is used to recover the displacement fields from the measured height profiles. The resulting three-dimensional displacements of the pad areas, see section 3.1, are translated to boundary conditions on the nodes of the pads in the model.

3. Results

In this section, the results of the analysis of the stretchable interconnect experiment are presented. First the displacements of the beams were determined using an isogeometric global digital height correlation method [35]. Furthermore, the integrated DHC method is tested by means of a virtual test. Finally, the real experiment is analyzed with the IDHC method.

3.1. Displacement field analysis with isogeometric digital height correlation

In order to obtain insight in the displacements of the beams, an isogeometric global DHC algorithm is employed. The

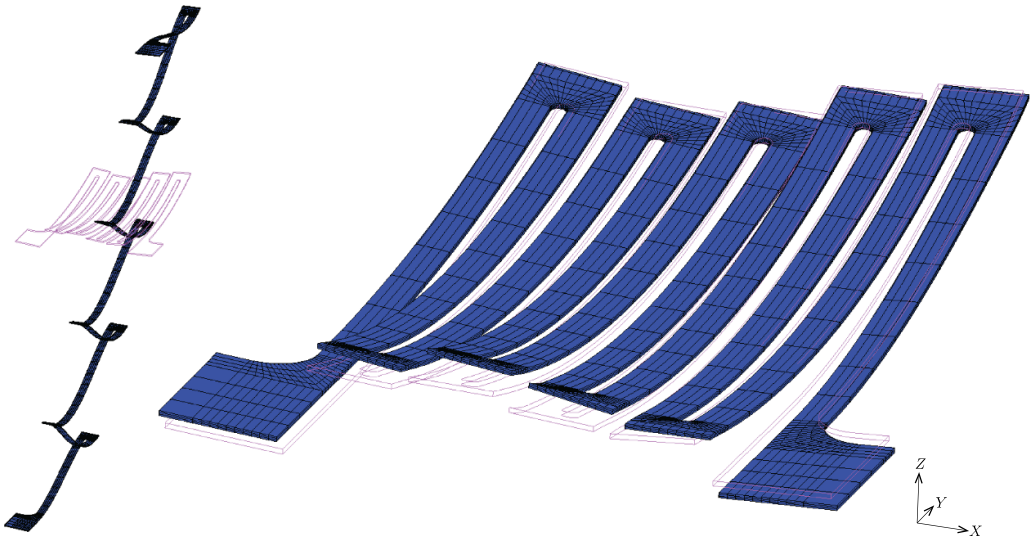

Figure 7. FE simulation of increment 8 in the experiment, where the boundary conditions in extended (left) and returned (right) state are derived from the measured topographies.

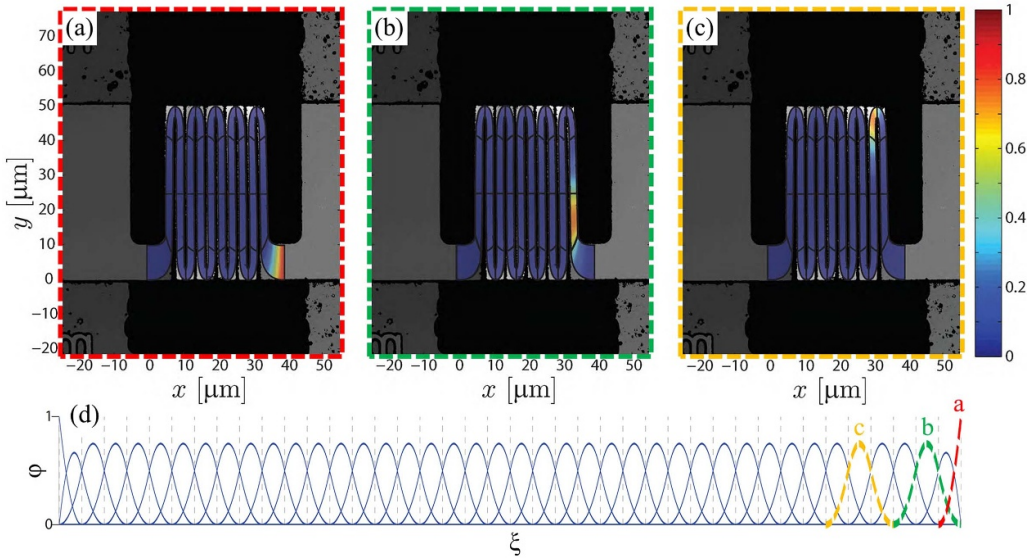

Figure 8. The mesh of NURBS shape functions used in the isogeometric *Global* DHC analysis of the three-dimensional displacement field of the stretchable interconnect, which is used to provide accurate displacement boundary conditions to the FEM simulations in the *integrated* DHC framework. The shape functions are second-order b-splines along the length of the interconnect, of which the one-dimensional representation is shown in the bottom figure (d), and zeroth order in the width direction, i.e. constant over the width. In total 42 two-dimensional shape functions are defined; the amplitude field of three 2D shape functions are shown in subfigures (a)–(c), which also show the mesh of the elements with black lines. The colored dashed lines around the subfigures indicate for each of the three shape functions to which one-dimensional second-order shape function along the interconnect length in (d) they correspond.

results can be used to validate the displacements calculated with the FE simulation after the parameter identification with IDHC. Moreover, the displacements of the clamping pads are essential to define boundary conditions in the FE model for the integrated height correlation. The technique used for this purpose is the isogeometric DHC algorithm introduced in [35], where NURBS shape functions are used for both the parametrization of the geometry and the discretization of the displacement field [46].

Because the regions between the beams are discontinuous, it is not possible to use a rectangular region of interest with a mesh of shape functions. Instead, a very long and narrow region of interest is needed that follows the meandering beam structure of the specimen. To mesh this region of interest, the commercial CAD software Autodesk AutoCAD[1] is used. The mesh consists of 40 elements along the total length of the interconnect, containing second-order shape functions, while in the width direction only one element is used with zeroth order shape functions, i.e. a constant value over the beam width.

[1] Autodesk. *AutoCAD software*: http://www.autodesk.com/products/autocad/overview.

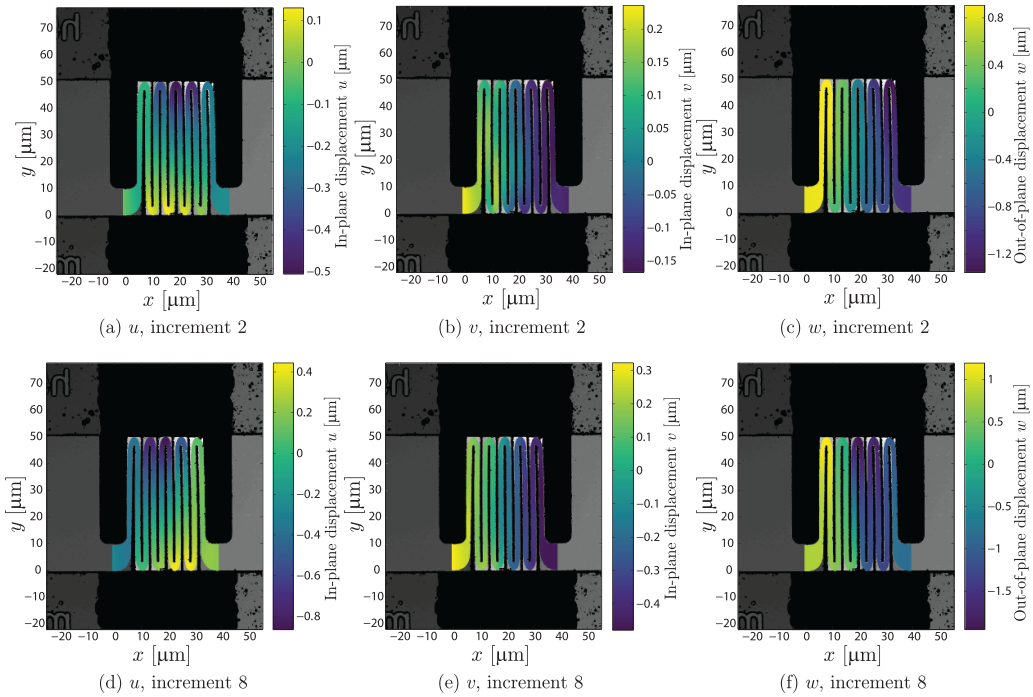

(a) u, increment 2 (b) v, increment 2 (c) w, increment 2

(d) u, increment 8 (e) v, increment 8 (f) w, increment 8

Figure 9. Calculated in-plane displacement fields u (in x-direction), v (in y-direction) and out-of-plane displacement field w for two loading increments in the experiment. The displacements are given in micrometers.

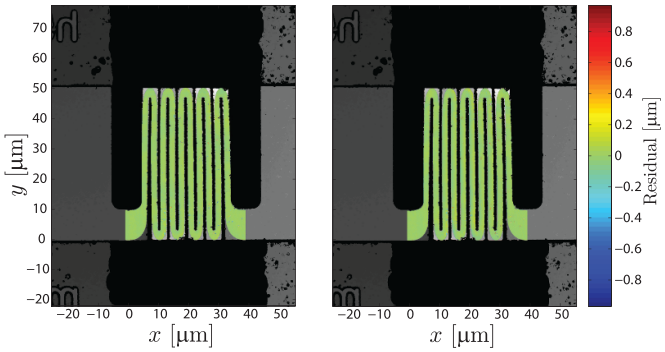

(a) Increment 2 (b) Increment 8

Figure 10. Residual images for the corresponding increments shown in figure 9.

Their product results in 42 two-dimensional functions for this geometry, see figure 8. For this experiment it is important to limit the number of degrees of freedom (and hence, shape functions), because the correlation sensitivity to local minima is high due to the limited quality of the height pattern (silica particles) and high acquisition noise, especially at the large boundary of the slender structure. Therefore, the number of elements along the length of the interconnect is taken as small as possible while still describing the geometry accurate enough. This choice disregards the outside corners of the hinges, which is acceptable as these corners do not deform anyway. Also the choice for zeroth order shape functions in the width direction of the beams limits the number of degrees of freedom, which is justified because the strain in width direction remains negligible due the long free side edges of the beams. Therefore, the proposed limited set of shape functions is able to fully capture the kinematics of the interconnect structure.

Another measure taken to prevent correlation to a local minimum is to supply an adequate initial guess. Therefore, the rigid body displacements of the clamping pads are estimated manually at pixel level from the topography images and interpolated linearly over the beams.

The resulting displacement fields are shown in figure 9 for one of the first and last increments in the experiment, which provide a good impression of the evolving plastic deformation after unloading at the end of each loading–unloading cycle. The figure shows that the major part of the three-dimensional displacement field for each increment is governed by the actual location of the clamps after unloading, which varies for each increment. Therefore, imposing this measured 3D clamp displacement as a boundary condition on the FE simulation in the IDHC routine is critical for obtaining convergence. Since the error in the displacement fields cannot be determined, as this is a real experiment and the true displacements are unknown, the only available measure for accuracy of the calculated displacements is the residual images, i.e. the difference between the reference image and the incremental (deformed) images back-deformed to the initial configuration using the calculated displacement fields. It can be seen in figure 10 that the residual is close to zero for the entire region of interest. Hence, it is concluded that the obtained displacements with DHC are reliable.

3.2. *IDHC parameter identification on virtual tests*

In order to assess the integrated digital height correlation framework for an experiment with the complexity of the

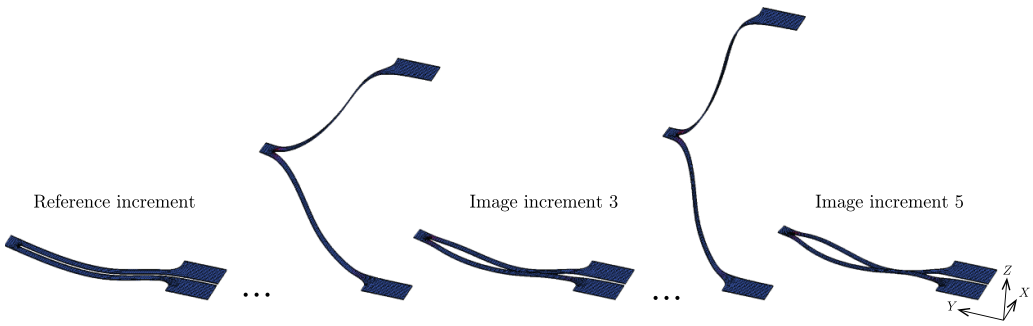

Figure 11. FE simulation for the virtual test case. The interconnect structure consists of two beams, of which one is lifted to a prescribed height and displaced back to the reference position a number of times, with increasing lifting height. The image increments are based on the returned configurations, as indicated in the figure for three increments (the dots indicate loading cycles not shown in this figure).

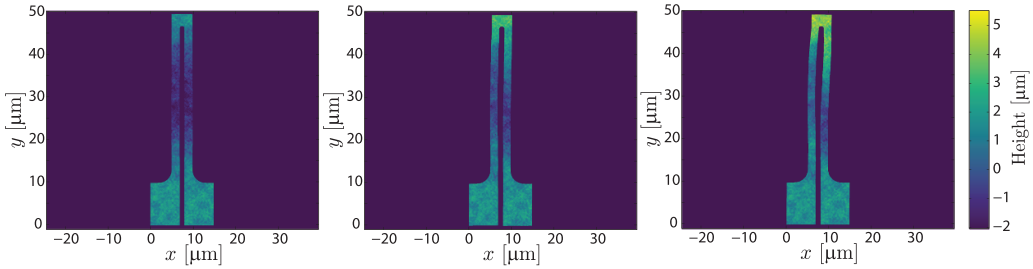

(a) f (b) g increment 3 (c) g increment 5

Figure 12. Topographies for the virtual test case to be analyzed with IDHC. Left, the topography of the reference configuration, f. The deformed topographies g of two of the five increments in the middle and on the right.

interconnect structure, a virtual test is executed first. In this numerical simulation, the images are created artificially from a finite element simulation and a synthetic reference image. In this virtual test case, a freestanding stretchable interconnect structure of two beams is modeled, which captures the main deformation modes occurring in the considered experiment on a 10-beam structure. Similar to the real experiment, one end of the interconnect is displaced in the out-of-plane direction by a prescribed distance, increasing over a number of cycles, and consecutively returned to its initial height position, see figure 11.

The simulation results, i.e. three-dimensional nodal displacements, are used to deform the synthetic reference topography that contains a computer generated height pattern, see figure 12(a), to create the deformed topographies, of which two are shown in figures 12(b) and (c).

In the FE model the same elasto-plastic material model with a rate power law hardening relation (equation (1)) is used. The objective of the IDHC correlation of the virtual test case is to recover the parameters in this model that are used to create the virtual test data, i.e. $\sigma_{y0} = 200 \times 10^{-6}$ N µm^{-2} (=200 MPa), $A = 6.43 \times 10^{-4}$ N µm^{-2} and $m = 0.2$. Therefore, this virtual test allows to assess the error sources affecting the IDHC parameter identification.

It is first noted that preliminary numerical simulations immediately demonstrated the importance of selecting a proper set of topographies: (a) a sufficient number of increments is required to find a unique solution for the three parameters in the numerical model and (b) increments should be far enough in the plastic regime to ensure sufficient sensitivity to the parameters. Based on this analysis, it was chosen to include five loading-unloading cycles (or increments) that all fall in the plastic regime, in the IDHC correlation, i.e. five deformed topographies and the reference topography.

To test the robustness of the IDHC correlation for identification of the three plasticity parameters on these six topographies, an initial guess relatively far from the solution is employed, of approximately three times higher values for all three parameters. This initial guess is based on the physical significance of the parameters. For the initial yield strength σ_{y0} a lower bound for a realistic range for the considered test specimen is set by the bulk value of aluminum, which is approximately 70 MPa. The upper bound is 700 MPa, indicating a strong strengthening effect due to miniaturization, which was visually determined in [26] by comparing images of a stretching experiment with these samples to numerical simulations with different values for the yield strength. The initial guess is chosen in the upper region of this range. The hardening parameters A and m are less determined for these specific specimen, but typical values for these parameters for metals and metal alloys range between 100–2000 MPa and 0.1–0.5 respectively. The initial guesses for these parameters are also in the upper region of this range. The convergence behavior is plotted in figure 13. The IDHC algorithm adequately converges towards the expected solution. The initial guess values and the resulting values, with their associated errors, are presented in table 1. This indicates that the algorithm is able to converge even relatively far from the solution, leading to accurate results with errors in the order of 10^{-3}.

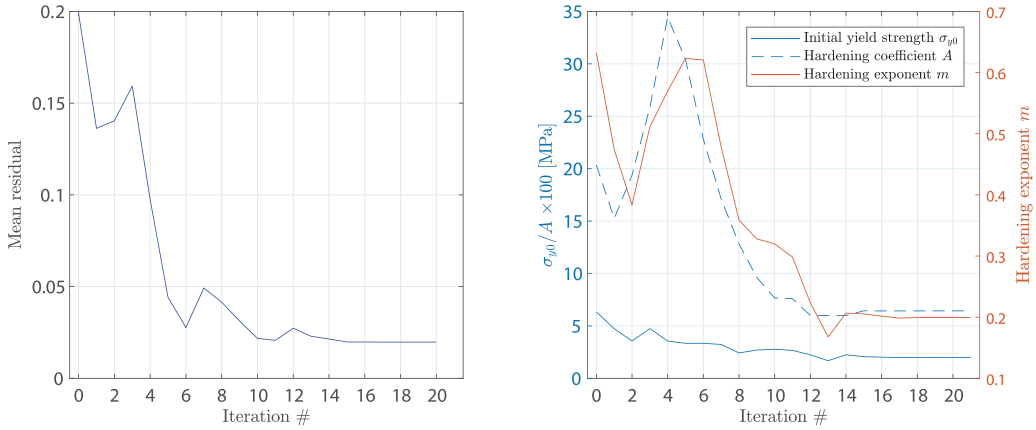

Figure 13. IDHC convergence for the virtual test case. The evolution of the mean value of the residual (averaged both spatially and over time) and of the three resolved parameters, σ_{y0}, A and m is depicted.

Table 1. Results for the parameter identification with IDHC for the virtual test with a two-beam stretchable interconnect. The initial guess on the parameters is listed, as well as the value resulting from the correlation and the error in the determined parameters.

Parameter			Initial guess	Identified value	Relative error[a]
Initial yield strength	σ_{y0}	(N µm^{-2})	632×10^{-6}	199×10^{-6}	3.5×10^{-3}
Hardening coefficient	A	(N µm^{-2})	2.04×10^{-3}	6.43×10^{-4}	3.1×10^{-4}
Hardening exponent	m	(—)	0.63	0.199	3.1×10^{-3}

[a] Relative error $=$ |Calculated value $-$ True value|/True value.

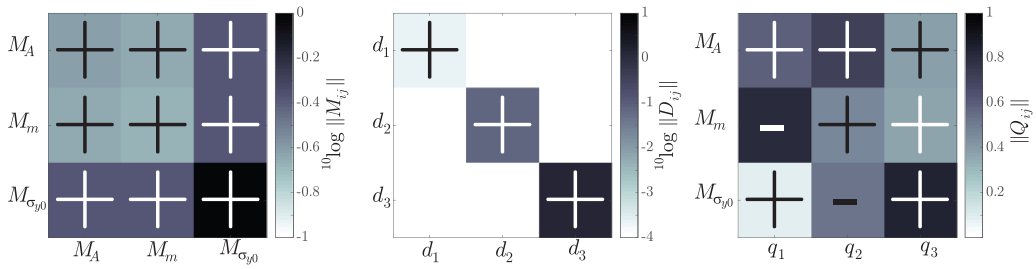

Figure 14. Graphical representation of the correlation matrix M and its spectral decomposition; eigenvalue matrix D and eigenvector matrix Q, which represent the sensitivity towards the three degrees of freedom (A, m and σ_{y0}). The symbol in each matrix component displays the sign of the corresponding value.

However, note that the convergence behavior is still oscillatory, even for this virtual test case where there are no error sources from experimental artifacts and discrepancies between the numerical model and the real world. This indicates that the problem is complex and difficult to correlate, which is also confirmed by the sensitivity analysis of the correlation matrix, see figure 14. In this sensitivity analysis a spectral decomposition is made from the correlation matrix M: $M = QDQ^{-1}$, with the columns of Q being the eigenvectors of M and D a diagonal matrix containing the eigenvalues. From the correlation matrix M itself it becomes clear that the sensitivity towards parameters A and m is much smaller than the sensitivity to σ_{y0}. Furthermore, the eigenvector matrix Q reveals cross-sensitivity between the parameters, especially between A and the other parameters. Although the algorithm works well for this numerical simulation, complications can be expected when additional experimental error sources come into play.

3.3. Parameter identification from a real 3D test on a freestanding stretchable interconnect

Finally, the IDHC algorithm is applied to the topographies of the real out-of-plane loading experiment of section 2.1, see figure 3. A set of increments is used, mainly towards the end of the experiment, to incorporate enough topographies where plasticity has a quantifiable effect. The correlation is first executed for all three parameters of the hardening model simultaneously. When the correlation is started from initial guesses covering the entire range of physically meaningful and expected values (i.e. $70 < \sigma_{y0} < 700$ MPa [26], $0.1 < m < 0.5$, $100 < A < 1000$ MPa), the correlation shows fast convergence towards the same broad global minimum, which demonstrates a high robustness of the IDHC framework against poor initial guesses, also for the experimental case.

Unfortunately, however, for none of the initial guesses true convergence of the parameters was reached, because

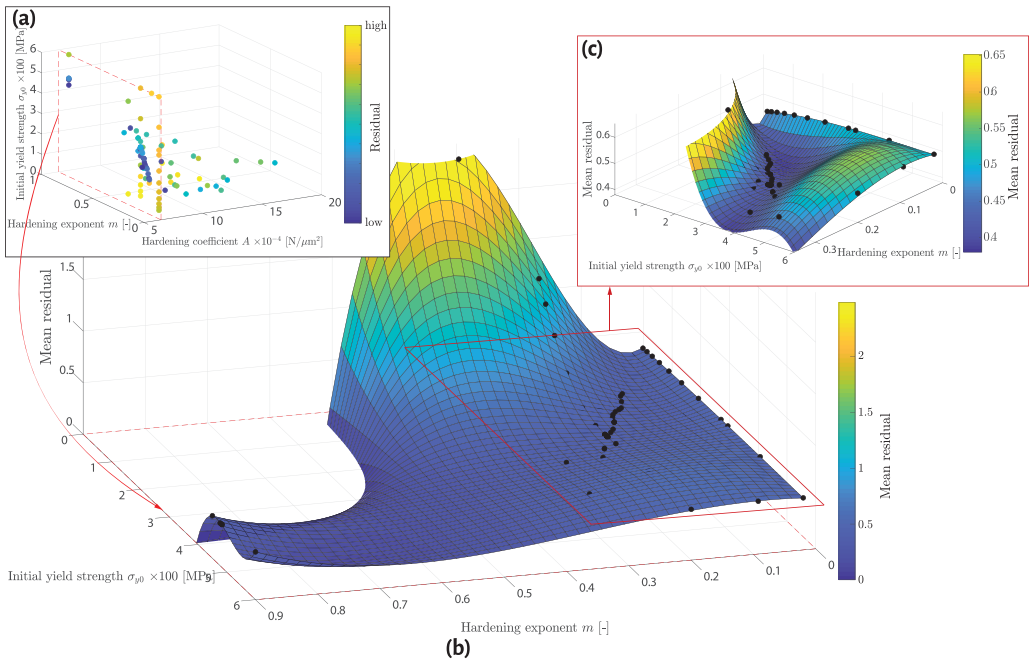

Figure 15. (a) Residual landscape as a function of the three parameters A, m and σ_{y0}. For visualization purposes, the colors indicate the *order* of the mean value of the residual from low to high, instead of their exact value. (b) Two-parameter cross section of the residual landscape, for A constant at 644 MPa, as indicated in (a) by a red dotted rectangle. A 3rd order polynomial surface is fit through the data (black markers) for visualization purposes. A zoom of this landscape is depicted in (c).

the algorithm continues to 'jump' up and down the valley, without finding the true global minimum. When looking at the non-convex residual landscape, see figure 15, it is observed that many local minima exist. However, all correlations converge to the same plane, i.e. the cross-section of the residual landscape where the hardening coefficient A is approximately 644 MPa. Furthermore, the residual landscape remains flat over a large region, which is especially clear from the fitted third-order polynomial surface through the $A \approx 644$ MPa cross-section in figure 15(b), with a broad valley around the values $\sigma_{y0} \approx 300$ MPa, $m \approx 0.2$, and $A \approx 644$ MPa and local fluctuations in the data, see figure 15(c). This broad valley filled with local minima explains the lack of convergence of the IDHC algorithm despite of its high robustness against poor initial guesses. The most important factor causing this effect is the low amount of plasticity occurring in the samples during the experiment, due to limitations in the experimental setup in terms of maximum achievable displacements with respect to the extreme stretchability of the samples, as explained in section 2.1. A low sensitivity towards the plasticity parameters reflected in the height profiles, and consequently the residuals, is the result. Other factors that likely play a role include experimental error sources, e.g. the limited pattern quality and measurement uncertainties in the topographies, defects in the sample that play an important role in the deformation mechanics, and also model errors, such as discrepancy in the exact geometry, especially the thickness that is not quantified precisely, and the material model itself. An isotropic plasticity model is used, while the small size of the specimen suspects columnar crystals with few grain boundaries inducing size effects that are better modeled with, e.g. a crystal plasticity framework with strain gradient dislocation density effects [47].

Next, the correlation is performed only for the initial yield strength σ_{y0}, while the values for A and m are fixed at the values in the apparent minimum, i.e. $m = 0.2$ and $A = 644$ MPa. The correlation is initiated from two different initial guesses: 70 MPa, which is the bulk material property for aluminum, and 600 MPa, which is in the range of (700 ± 100) MPa as was estimated in [26] for the considered interconnects. The convergence plot is shown in figure 16, where the decrease in the residual becomes apparent, as well as the convergence of the parameter σ_{y0} towards the same value from both initial guesses. The resulting initial yield strength is approximately 300 MPa. This is much smaller than the in [26] estimated value of (700 ± 100) MPa, where only a qualitative manual comparison between experiment and an unrefined numerical model was made. However, it is significantly higher than the value for bulk aluminum, and hence, still indicates a strong strengthening effect due to the sub-micron dimension (thickness) of the interconnect. Also, if the result of the numerical simulation for the correlated initial yield strength of 300 MPa and for both the initial guesses is compared to the experimental height profile, see right image in figure 16, it is observed that the deformed shape is indeed adequately approximated after IDHC. Yet, in the finite element model a choice was here made for the other two material parameters that describe the plastic regime, hardening coefficient A and exponent m. The choice of these values might induce a model error and affect the resulting value for the initial yield strength.

In order to evaluate the accuracy of the determined initial yield strength, the correlation is repeated for different

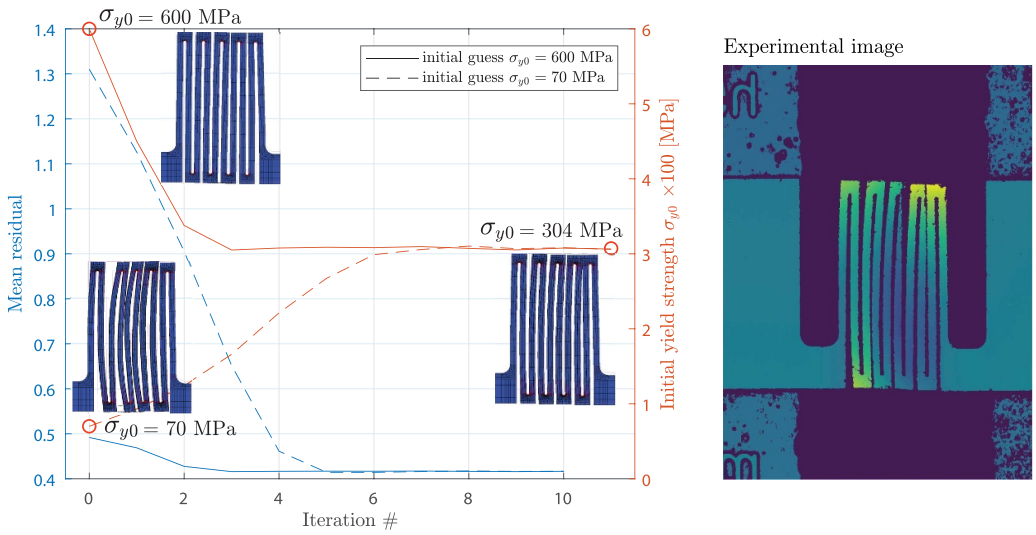

Figure 16. Convergence for the correlation of the initial yield strength parameter σ_{y0}. The evolution of the mean value of the residual (averaged both spatially and over time) and of σ_{y0} is depicted. Furthermore, the deformed geometry from the numerical simulations is shown for the two different initial guesses (i.e. 70 and 600 MPa) as well as for the correlated value of 304 MPa at the final IDHC increment. For comparison the measured height profile of the deformed geometry from the same load cycle is depicted as well, which show good agreement with the deformed geometry simulated for 304 MPa.

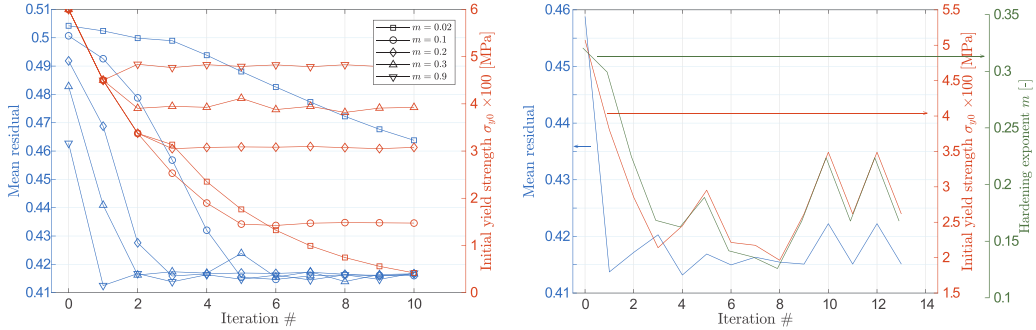

(a) Convergence for correlation of σ_{y0}, m fixed

(b) Convergence for correlation of σ_{y0} and m simultaneously

Figure 17. (a) Convergence for the correlation of the initial yield strength parameter σ_{y0}, from an initial guess of 600 MPa and different values for the hardening exponent m, ranging from 0.02 (almost pure plasticity) to 0.9 (extreme hardening). (b) Convergence for the simultaneous correlation of σ_{y0} and m. The evolution of the mean value of the residual and the correlation parameters are depicted.

values of m, while A is kept constant at 644 MPa. Because this appears to be the cross-section with the lowest residual values in figure 15, it seems safe to assume that this value of the hardening coefficient is most likely the true value. It is observed in figure 17(a) that the yield strength converges towards different values for different choices for m and that the residual for all these cases is approximately the same. This is consistent with the valley that appears in the residual landscape of figure 15 and indicates cross-sensitivity between the parameters. Only the case of almost pure plastic behavior, with low hardening ($m = 0.02$) seems to converge worse than the other cases, so it is expected that these values of the yield strength and hardening exponent form a lower bound.

Next, correlation for both the initial yield strength and the hardening exponent is performed simultaneously, see figure 17(b), where A is again fixed at 644 MPa. The residual decreases to roughly the same value as for the other correlations, while significant fluctuations are noticed. The lowest residual value indicates that the best fit for the parameters is an initial yield strength of approximately 225–300 MPa, with a hardening exponent of around 0.15–0.2. The ranges are estimated by comparing the parameter values at the absolute lowest residual value and the value towards the algorithm seems to converge in figure 17(b). Based on the three-dimensional residual landscape of figure 15(a), the true value of hardening coefficient A is estimated to be in the range of 600–800 MPa. Although the accuracy of the identification is modest, the adopted procedure still indicates that parameter identification is possible with the IDHC method and more accurate results are expected upon improvement of the experiment and model.

4. Conclusions

The mechanical properties of a freestanding aluminum stretchable electrical interconnect have been analyzed by applying an

integrated digital height correlation method to topographies measured *in-situ* during a 3D experiment. The design of the interconnect allows for full three-dimensional deformations, e.g. large rotations and displacements, thereby enabling ultra-stretchability. This complicates the application of commonly used DIC methods for characterization, as the surfaces are required to stay in view during the deformation process and displace in-plane only. Therefore, a digital *height* correlation method was employed, in which the three-dimensional surface displacements can be tracked. An integrated approach was followed, where the correlation of the images is complemented by a finite element model, in which the parameters are unknowns. Moreover, the experiment was designed such that the surfaces remain in view: the specimen is loaded in the out-of-plane direction, thereby triggering the main deformation mode of the stretchable interconnect, i.e. bending of its beam members.

It is of utmost importance that the boundary conditions applied in the finite element model comply with those in the experiment. Therefore, the experimental data was first analyzed using a global DHC method. The displacements of the clamping pads were identified and used in the numerical model. Also, the initial geometry of the interconnect was established from the reference image and translated to the model, as the as-processed interconnect already has a warped configuration due to relaxed residual stresses from manufacturing, influencing the deformations and inducing model errors when not taken into account.

A virtual test was first executed to verify the IDHC algorithm. The stretchable interconnect geometry was implemented, along with a power law hardening model with three parameters, which were the objective for identification. It was shown that even for large mismatches in the initial values, the method converged towards the correct solution with an error in the resulting parameters in the order of 10^{-3}. However, it was also shown that even in this case without experimental uncertainties and model errors, the convergence path was irregular, indicating the complexity of this parameter identification problem. This was also confirmed by a sensitivity analysis of the correlation matrix, which showed large differences in sensitivity towards the individual parameters and also cross-sensitivity between the parameters.

Finally, the real experiment was analyzed. For simultaneous correlation of all three plasticity model parameters , robust convergence towards the same global valley was found, demonstrating high robustness of the IDHC framework against poor initial guesses, also for the experimental case. Unfortunately, however, convergence to the true global minimum was never reached, the reason for which was identified to be the non-convex residual landscape containing a broad valley with many local minima. It appeared extremely challenging to obtain a sufficient amount of plasticity in the experiment, due to the combination of very compliant interconnect structures, that are designed to stretch elastically in a large range, with an experimental setup that needs nanometer precision, while the trade-off is limited actuation range. Additionally, plasticity in the samples needs to be translated to visual deformation in captured height maps, which suffer from acquisition noise and limited resolution due to the micron-sized dimensions of the interconnects. Visual deformation in these images could either correlate to true plastic behavior, but also to deviations in the unloaded clamping pad positions, enhanced by the initial curvature of the interconnect beams due to residual stresses. To guide correlation, a multi-step approach was followed. First, the initial yield strength was correlated with the two other parameters fixed. From two different initial guesses the value converged to approximately 300 MPa, which is significantly higher than the value for bulk aluminum and indicates a strong strengthening effect due to miniaturization of the interconnects, for which the most occurring mechanisms are strain gradients [7, 8], dislocation starvation [7, 48] and constrained boundary layers [7]. However, this value is significantly lower than the value of 700 MPa, which was determined in [26] by visually comparing simulation results for different yield strengths to experimental images. It was observed in the current work that it is extremely difficult to visually distinguish true plastic behavior from other effects that lead to visual deformations and that a highly sensitive algorithm is needed to identify plasticity. This explains the difference between the initial yield strength value found here and in [26]. The choice made for the other two parameters in the hardening model still influenced the actual value of the correlated parameter. Repeating the correlation for different values of the hardening exponent indeed revealed convergence of the initial yield strength to different values. Subsequently the initial yield strength and hardening exponent were correlated simultaneously. Despite the moderate accuracy of the identification, the initial yield strength was estimated at 225–300 MPa and the hardening exponent at 0.15–0.2. The hardening coefficient was assumed 644 MPa, which appeared to yield the lowest residual in the three-dimensional landscape.

The results show that the IDHC technique is suitable for parameter identification in the challenging case of real three-dimensional experiments on micron-scale freestanding stretchable interconnects. Minimal changes in the height maps, for which with the bare eye it cannot be distinguished if they originate from plasticity or from clamping pad displacements combined with initial curvature, are extracted with the IDHC algorithm and lead to a reasonable estimate of the plasticity parameters. This indicates the extreme sensitivity of the method. To increase the accuracy of the identification it is recommended to improve the experimental settings and to advance the numerical model in order to diminish as many error sources as possible. E.g., the applied height pattern is object for improvement, the geometry of the interconnect could be modeled more precisely and a material model including dislocation density strain gradient crystal plasticity could be used. This is, however, beyond the scope of the present work, where potency of the IDHC technique was shown and a first estimate of the material parameters for an isotropic hardening plasticity model was determined.

Acknowledgment

The research was funded by the Netherlands Organization for Scientific Research (NWO) under the VIDI scheme (project number STW12966).

ORCID iD

J P M Hoefnagels https://orcid.org/0000-0001-8359-7575

References

[1] Xu L *et al* 2014 3D multifunctional integumentary membranes for spatiotemporal cardiac measurements and stimulation across the entire epicardium *Nat. Commun.* **5** 3329
[2] Someya T 2012 *Stretchable Electronics* (New York: Wiley)
[3] Klinker L *et al* 2015 Balloon catheters with integrated stretchable electronics for electrical stimulation, ablation and blood flow monitoring *Extreme Mech. Lett.* **3** 45–54
[4] Schiavone G and Lacour S P 2019 Conformable bioelectronic interfaces: mapping the road ahead *Sci. Trans. Med.* **11** eaaw5858
[5] Uchic M D, Schade P A and Dimiduk D M 2009 Plasticity of micrometer-scale single crystals in compression *Annu. Rev. Mater. Res.* **39** 361–86
[6] Kraft O, Gruber P A, Mönig R and Weygand D 2010 Plasticity in confined dimensions *Annu. Rev. Mater. Res.* **40** 293–317
[7] Greer J R and De Hosson J 2011 Plasticity in small-sized metallic systems: intrinsic versus extrinsic size effect *Prog. Mater. Sci.* **56** 654–724
[8] Fleck N A, Muller G M, Ashby F and Hutchinson J W 1994 Strain gradient plasticity: theory and experiment *Acta Metall. Mater.* **42** 475–87
[9] Yu X, Majahan B K, Shou W and Pan H 2017 Materials, mechanics and patterning techniques for elastomer-based stretchable conductors *Micromachines* **8** 7
[10] McCoul D, Hu W, Gao M, Mehta V and Pei Q 2016 Recent advances in stretchable and transparent electronic materials *Adv. Electron. Mater.* **2** 1500407
[11] Chtioui I, Bossuyt F, Vanfleteren J and Bedoui M H 2018 2.5/3D dynamically stretchable and permanently shaped electronic circuits *Microsyst. Technol.* **24** 831–53
[12] Yao S and Zhu Y 2015 Nanomaterial-enabled stretchable conductors: strategies, materials and devices *Adv. Mater.* **27** 1480–1511
[13] Ahn J H and Je J H 2012 Stretchable electronics: materials, architectures and integrations *J. Phys. D: Appl. Phys.* **45** 103001
[14] Khang D-Y, Jiang H, Huang Y and Rogers J A 2006 A stretchable form of single-crystal silicon for high-performance electronics on rubber substrates *Science* **311** 208–12
[15] Kim D-H *et al* 2008 Materials and noncoplanar mesh designs for integrated circuits with linear elastic responses to extreme mechanical deformations *Proc. Natl Acad. Sci.* **105** 18675–80
[16] Jackman R J, Brittain S T, Adams A, Prentiss M G and Whitesides G M 1998 Design and fabrication of topologically complex, three-dimensional microstructures *Science* **280** 2089–91
[17] Gonzalez M, Axisa F, Vanden Bulcke M, Brosteaux D, Vandevelde B and Vanfleteren J 2008 Design of metal interconnects for stretchable electronic circuits *Microelectron. Reliab.* **48** 825–32
[18] Plovie B, Vanfleteren J, Vervust T, Quintero A V and Bossuyt F 2019 Design automation of meandered interconnects for stretchable circuits *IEEE Trans. Comput. Aided Des. Integr. Circuit Syst.* **38** 1648–60
[19] Gray D S, Tien J and Chen C S 2004 High-conductivity elastomeric electronics *Adv. Mater.* **16** 393–7
[20] Su Y, Wang S, Huang Y, Luan H, Dong W, Fan J A, Yang Q, Rogers J A and Huang Y 2015 Elasticity of fractal inspired interconnects *Small* **11** 367–73
[21] Ma Q and Zhang Y 2016 Mechanics of fractal-inspired horseshoe microstructures for applications in stretchable electronics *J. Appl. Mech.* **83** 111008
[22] Silverberg J L, Evans A A, McLeod L, Hayward R C, Hull T, Santangelo C D and Cohen I 2014 Using origami design principles to fold reprogrammable mechanical metamaterials *Science* **345** 647–50
[23] Shi Y *et al* 2017 Plasticity-induced origami for assembly of three dimensional metallic structures guided by compressive buckling *Extreme Mech. Lett.* **11** 105–10
[24] Collins G P 2016 Science and culture: kirigami and technology cut a fine figure, together *Proc. Natl Acad. Sci.* **113** 240–1
[25] Tang Y and Yin J 2017 Design of cut unit geometry in hierarchical kirigami-based auxetic metamaterials for high stretchability and compressibility *Extreme Mech. Lett.* **12** 77–85
[26] Shafqat S, Hoefnagels J P M, Savov A, Joshi S, Dekker R and Geers M G D 2017 Ultra-stretchable interconnects for high-density stretchable electronics *Micromachines* **8** 277
[27] Hild F and Roux S 2006 Digital image correlation: from displacement measurement to identification of elastic properties—a review *Strain* **42** 69–80
[28] Réthoré J 2010 A fully integrated noise robust strategy for the identification of constitutive laws from digital images *Int. J. Numer. Methods Eng.* **84** 631–60
[29] Neggers J, Hoefnagels J P M, Geers M G D, Hild F and Roux S 2015 Time-resolved integrated digital image correlation *Int. J. Numer. Methods Eng.* **103** 157–82
[30] Niu Y, Wang J, Shao S, Wang H, Lee H and Park S B 2018 A comprehensive solution for electronic packages reliability assessment with digital image correlation (DIC) method *Microelectron. Reliab.* **87** 81–8
[31] Han K, Ciccotti M and Roux S 2010 Measuring nanoscale stress intensity factors with an atomic force microscope *EPL Europhys. Lett.* **89** 66003
[32] Bergers L I J C, Hoefnagels J P M and Geers M G D 2014 Characterization of time-dependent anelastic microbeam bending mechanics *J. Phys. D: Appl. Phys.* **47** 1–14
[33] Neggers J, Hoefnagels J P M, Hild F, Roux S and Geers M G D 2014 Direct stress-strain measurements from bulged membranes using topography image correlation *Exp. Mech.* **54** 717–27
[34] Shafqat S, van der Sluis O, Geers M G D and Hoefnagels J P M 2018 A bulge test based methodology for characterizing ultra-thin buckled membranes *Thin Solid Films* **660** 88–100
[35] Kleinendorst S M, Hoefnagels J P M, Fleerakkers R C, van Maris M P F H L, Cattarinuzzi E, Verhoosel C V and Geers M G D 2016 Adaptive isogeometric digital height correlation: application to stretchable electronics *Strain* **52** 336–54
[36] Bertin M, Du C, Hoefnagels J P M and Hild F 2016 Crystal plasticity parameter identification with 3D measurements and integrated digital image correlation *Acta Mater.* **116** 321–31
[37] Shafqat S, Savov A M, Joshi S, Dekker R, Geers M G D and Hoefnagels J P M 2020 Multi-axial electro-mechanical testing methodology for highly stretchable freestanding

micron-sized structures *J. Micromech. Microeng.* **30** 055002
[38] Ruybalid A P, Hoefnagels J P M, van der Sluis O and Geers M G D 2018 Image-based interface characterization with a restricted microscopic field of view *Int. J. Solids Struct.* **132–133** 218–31
[39] Rokoš O, Hoefnagels J P M, Peerlings R H J and Geers M G D 2018 On micromechanical parameter identification with integrated DIC and the role of accuracy in kinematic boundary conditions *Int. J. Solids Struct.* **146** 241–59
[40] Scrivens W A, Luo Y and Sutton M A 2006 Development of patterns for digital image correlation measurements at reduced length scales *Exp. Mech.* **47** 63–77
[41] Dong Y L and Pan B 2017 A review of speckle pattern fabrication and assessment for digital image correlation *Exp. Mech.* **57** 1161–81
[42] Hoefnagels J P M, van Maris M P F H L and Vermeij T 2019 One-step deposition of nano-to-micron-scalable, high-quality digital image correlation patterns for high-strain *in-situ* multi-microscopy testing *Strain* **55** e12330
[43] Bruck H A, McNeill S R, Sutton M A and Peters III W H 1989 Digital image correlation using Newton–Raphson method of partial differential correction *Exp. Mech.* **29** 261–7
[44] Neggers J, Blaysat B, Hoefnagels J P M and Geers M G D 2015 On image gradients in digital image correlation *Int. J. Numer. Methods Eng.* **105** 243–60
[45] Fenner R T 1999 *Mechanics of Solids* (Boca Raton, FL: CRC Press)
[46] Kleinendorst S M, Hoefnagels J P M, Verhoosel C V and Ruybalid A P 2015 On the use of adaptive refinement in isogeometric digital image correlation *Int. J. Numer. Methods Eng.* **104** 944–62
[47] Evers L P, Brekelmans W A M and Geers M G D 2004 Scale dependent crystal plasticity framework with dislocation density and grain boundary effects *Int. J. Solids Struct.* **41** 5209–30
[48] Greer J R and Nix W D 2006 Nanoscale gold pillars strengthened through dislocation starvation *Phys. Rev.* B **73** 245410